ACADEMIA
MATERIALS SCIENCE

Research Article
Published: 2025-04-01
https://doi.org/10.20935/AcadMatSci7591

Hybrid model of hydrogen thermal desorption from structural materials

Yury V. Zaika[1,*], Ekaterina K. Kostikova[1]

Academic Editors: Raul D.S.G. Campilho

Abstract

To solve problems of hydrogen power engineering, there is an intensive search for materials for hydrogen storage. Thermal desorption spectrometry (TDS) is one of the effective experimental methods for studying the interaction of structural materials with hydrogen isotopes. A sample (we consider a thin plate made of a material with metallic properties) pre-saturated with dissolved atomic hydrogen is heated relatively slow in a vacuum chamber. The degassing flux is registered using a mass spectrometer. The spectrum is the dependence of the desorption flux density from a two-sided surface of the sample on the current temperature. Quite often, several local peaks are registered on the spectrum. Traditionally, this is associated with the reversible capture of various kinds of traps (inhomogeneities of the material) with different binding energies. However, numerical experiments on models with dynamic boundary conditions describing the dynamics of surface concentrations show the possibility of a different scenario. The following scheme is possible: The first peak occurs when hydrogen leaves the surface and the subsurface volume. Then, a large concentration gradient is formed at the surface. For this reason, and during continued heating, diffusion influx from the volume is significantly activated, which leads to the next peak of desorption. Recommendations on how to distinguish degassing scenarios corresponding to these essentially different physicochemical reasons are given. This is fundamentally important for the correct recalculation of modeling results from laboratory samples to real constructions. The hybrid thermal desorption model can be considered as a computational algorithm for solving a partial differential system using an approximation by an ODE system (but this is not a straight-line method).

Keywords: *hydrogen interaction with solids, surface processes, thermal desorption, dynamical boundary value problems, computer simulation*

Citation: Zaika YV, Kostikova EK. Hybrid model of hydrogen thermal desorption from structural materials. *Academia Materials Science* 2025;2. https://doi.org/10.20935/AcadMatSci7591

1. Introduction

Green hydrogen has been increasingly recognized as a critical solution for decarbonization [1–4]. It is sufficient to operate with volume-averaged concentrations for many applied problems. This is quite adequate for porous, powdery materials, when the sample geometric characteristics are unimportant. We will consider the models in the context of the thermal desorption spectrometry (TDS) experimental method. For definiteness, the authors focus on the capabilities of the experimental equipment described in detail in [5, 6]. A sample of the material pre-saturated with dissolved hydrogen is slowly heated under vacuum conditions. The density of the degassing flux is determined using a mass spectrometer. Let us narrow down the research object. The sample is a plate made of a test material with metallic properties (alloy). One can select the volume and the double-sided surface (we neglect the ends). Hydrogen dissolves in the atomic state. This is typical for materials in the applied task of producing extremely pure hydrogen based on membrane technologies. It can also be a material for storage systems and protection constructions in reactors (in long-term and thermonuclear ones). In real time, the experiment can be performed on thin plates, extrapolating the results to the walls (layers) of real structures next. At the same time, it is important to argue for the uniqueness of parameters' estimates with sufficient accuracy (depending on the task) for correct recalculation. Varying the heating law allows modeling the dehydrogenation flux, for example, of a hydride material in a car fuel tank. A mathematical model and computational algorithm for describing TDS dehydrogenation of powder are presented in [7]. In this case, the model becomes significantly more complicated (Stefan-type boundary value problem), since it is necessary to take into account the free (moving) boundary of the phase transition.

The main object of this paper is to present a hybrid model for the numerical simulation of hydrogen thermal desorption, combining a model in terms of volume-averaged concentration with a more detailed model in the form of a diffusion equation with nonlinear dynamic boundary conditions reflecting processes on the surface. As a result, we obtain a system of ordinary differential equations. This system has a relatively low order. The model does not require the development of specialized software. The presented model allows us to numerically simulate various situations and operating conditions of the material in any mathematical package without significant expenditure of computed machine time. The authors

---

[1] Institute of Applied Mathematical Research, Karelian Research Centre, Petrozavodsk, Russian Academy of Sciences, 185910 Petrozavodsk, Russia.
[*] email: zaika@krc.karelia.ru

used the free distributed package *Scilab*, the programming language of which practically coincides with *Matlab*. TDS Simulator for *Matlab* is presented in [8].

For the more complex model presented in Section 4, we had to develop our own software. Commercial mathematical packages do not yet have the corresponding software procedures. The fact is that the boundary value problem considered there has non-standard nonlinear dynamic boundary conditions. This leads to the appearance of fractional derivatives, which characterize the so-called dynamic systems with memory (actively studied in applied mathematics in recent times).

In accordance with this paper's objective, the authors do not provide a full literature review in the introduction. Reviews are presented in detail in the cited literature. All relevant material is presented sequentially with the appropriate references throughout. This is carried out intentionally so that the reader can holistically comprehend the preparatory argumentation and the detailed conclusion of the final hybrid model and computational scheme.

2. A model of reaction order $\alpha \in [1,\ 2]$

2.1. Diffusion limitation

The classic result is as follows [9, 10]. The sample is a thin plate; the ends are neglected in the process of degassing. In the volume, we consider the following diffusion equation:

$$\frac{\partial c}{\partial t} = \frac{\partial}{\partial x}\Big(D\frac{\partial c}{\partial x}\Big) = D(T)\frac{\partial^2 c}{\partial x^2}, \quad x \in [0, \ell].$$

Here, ℓ is the thickness of the plate, and for the diffusion coefficient, $D = D(T(t)) \equiv D[t]$ is performed, i.e., heating is slow and uniform (T does not depend on x). We will also use the sign of identity both as a designation and as an equality by definition. Usually, linear heating is used. The heating rate in the experiment is constant β ($[\beta] = \mathrm{K/s}$): $T(t) = T_0 + \beta t$. Upon reaching a certain maximum temperature $T_{\max}$, further heating discontinues ($T = T_{\max}$, $t > t_{\max}$). This may be intentional or due to the risk of overheating of the structure.

A boundary value problem is considered when degassing is strictly limited by diffusion: $c_t = D(T(t))c_{xx}$ $[t > 0, x \in (0, \ell)]$, $c = c_0 > 0$ $[t = 0]$, and $c = 0$ $[t > 0, x = 0, \ell]$ ($[c] = 1_{\mathrm{H}}/\mathrm{cm}^3$).

For the variable

$$X(t) \approx \frac{1}{\ell}\int_0^\ell c(t,x)\,dx\ \big(= \bar{c}(t)\big) \tag{1}$$

the approximate linear model (see [11] for more details) is obtained

$$\dot{X}(t) = -K(T)X(t), \quad X(0) = c_0 \quad \big([\dot{X}(t)] = 1/\mathrm{cm}^3\mathrm{s}\big),$$
$$K(T) = \pi^2\ell^{-2}D(T), \qquad T = T(t)\ (= T_0 + \beta t).$$

The value of $X(t)$ has meaning of the volume-averaged concentration of the dissolved hydrogen remaining in the sample at $t > 0$. The model is functional when the temperature is high enough (to neglect the rapid processes of dissolution and desorption on the surface), and we are interested in the integral flux of degassing without detailing the physicochemical processes. The model takes the form of a first-order reaction. In this case, the kinetic coefficient $K(T)$ is proportional to $D(T)$. This makes it possible to focus on the data on the diffusion coefficient for an experimental material and postulate the Arrhenius dependence on temperature: $K(T) = K_0 \exp\{-Q/[RT]\}$.

The degassing flux density $w(t) = -\dot{X}(t)$ is of interest. Here, we assume $1 = 1_{\mathrm{H}}$ for uniformity, although hydrogen is desorbed in molecular form (extreme temperatures are not considered). Due to the one-to-one correspondence $t \leftrightarrow T(t)$ during monotonic heating, it is possible to construct a graph $w(T)$ in the $\{T, w\}$ axes. This is the very TDS spectrum that serves as the input information for further analysis. If heating is stopped, then we further operate with the graph $w(t)$, $t > t_{\max}$. Usually, pressure is measured, but here we will not specify how these data are converted into flux. This is determined by the specific features of the experimental apparatus. This paper deals with the hybrid model; hence, the $w(T)$ graph is regarded as experimental data. The value of the initial uniform saturation c_0 is determined at the end of degassing (based on the integral of w) and the geometry of the sample.

Remark 1: It can be additionally normalized to the initial concentration: $\tilde{X} = X/c_0$, $\tilde{X}(0) = 1$. The ODE will remain unchanged (a linear homogeneous equation with the same coefficient $K(T)$) but the dimensionless variable $\tilde{X}(t)$ will already have the meaning of the remaining fraction of c_0. It is possible to operate over the desorbed fraction $Y(t) = 1 - \tilde{X}(t)$, and then $\dot{Y}(t) = K(T)(1 - Y(t))$, $Y(0) = 0$, $\widetilde{w}(t) = \dot{Y}(t)$, and $w(t) = \widetilde{w}(t)c_0$. Note that such a simple model, when strictly limited only by diffusion, does not react to c_0, but reacts to the geometric parameter ℓ: $K(T) = K(T; \ell)$. In nonlinear models, for the reasons listed below, we will not normalize to the initial concentration (unlike [11]) but will instead operate with the average concentration in accordance with **(1)**.

2.2. Limitation by desorption

It is assumed that with strict limitation of desorption in the volume, the concentration is almost uniform: $c(t, x) \approx c(t) \Rightarrow X(t) \approx c(t)$. Then, for reasons of material balance, we can write $\ell\dot{X} = -2b(T)X^2$, $X(0) = c_0$, and consider $b = b_0 \exp\{-E_b/RT\}$ as the effective recombination coefficient [12] (p. 52). The factor 2 emphasizes that desorption occurs from both surfaces (near-surface volumes) of the plate. The quadrate responds to the combination of two atoms into hydrogen molecules in the desorption process.

The distribution of concentration $c(t, x)$ is symmetric with respect to the centre of the plate $x = \ell/2$. Approximation $c(t, x) \approx c(t)$ is quite acceptable for thin samples with relatively large D (for membrane technologies). This applies to the case in which the reaction $\mathrm{H} + \mathrm{H} = \mathrm{H_2}$ is strictly limiting, which according to the laws of chemical kinetics leads to a second-order reaction model. For consistency, we consider the density of the volume-averaged degassing flux in atoms: $w(t) = -\dot{X}(t)$, $[w] = 1_{\mathrm{H}}/(\mathrm{cm}^3\mathrm{s})$. Thus, the value $J(t) = b(T)X^2(t)$ can be interpreted as the desorption flux from a surface unit (two-sided): $\ell w(t) = 2J(t)$, $[J] = 1/\mathrm{cm}^2\mathrm{s}$ and $[b] = \mathrm{cm}^4/\mathrm{s}$.

Remark 2: This is the second considered extreme case when diffusion is relatively fast and strictly limited only by desorption. Here, the kinetic coefficient is $K(T) = 2b(T)/\ell$. Instead of $D(T)$, $b(T)$ naturally appears, and the dependence on ℓ remains. If we turn to fractions $\tilde{X} = X/c_0$, then $d\tilde{X}/dt = -\tilde{K}\tilde{X}^2$, $\tilde{X}(0) = 1$, and $\tilde{K} = \tilde{K}(T; \ell, c_0) = 2b(T)c_0/\ell$. An additional dependence on the initial saturation appears. This has to be taken into account for metals and alloys. For porous powdery materials, the dependence of the kinetic coefficient on c_0, ℓ, should not be significant. In this case, one can formally write the second-order reaction equation as $d\tilde{X}/dt = -\tilde{b}(T)\tilde{X}^2$, interpreting $\tilde{b}(T)$ in this notation as a coefficient of averaged volume desorption. For these reasons, we leave the averaged volume concentration $X(t)$ as a variable, and leave the value c_0 in the initial data: $X(0) = c_0$.

2.3. Averaging over diffusion and desorption processes

In a wide range of experimental conditions, diffusion and desorption from the surface are essentially interdependent. The dynamics of processes on the surface dictates the boundary conditions for the diffusion equation.

Synthesising the above reasoning, let us consider the averaged model, taking into account linear uniform heating $T(t) = T_0 + \beta t$ $(dT = \beta dt)$. By virtue of $t \leftrightarrow T$, instead of $X(t)$ we can write $X(T)$ $(\approx \bar{c}(T))$ and

$$\frac{dX}{dT} = -\frac{K(T)}{\beta} X^{\alpha}(T), \quad X(T_0) = c_0,\ \alpha \in [1,2], \tag{2}$$
$$K(T) = K_0 \exp\{-Q[RT]^{-1}\},\ T \in [T_0, T_*],\ T_* < T_{\max}.$$

The parameter $\alpha \in [1,2]$ allows us to take into account the degree of participation of limiting factors. We apply averaging not only by concentration, but also by diffusion and recombination processes. The coefficient $K(T)$ indirectly depends on the fixed parameters α, ℓ. So, at $\alpha \sim 1$ we focus on $\pi^2\ell^{-2}D(T)$. And for value $\alpha \sim 2$, we use the coefficient $2b(T)/\ell$.

This model was analyzed analytically in the paper [11]. This paper specifically and additionally considered the normalization $X \to X/c_0 \in (0,1)$, $t > 0$, and only the temperature dependence $K(T)$. Kissinger's methodology for estimating K_0, Q from experiments with different heating rates was presented. The procedure for estimation from a single heating rate was also described.

Remark 3: In [13], a wide range of models $\dot{X} \equiv dX/dt = K(T)f(X)$, where $X(t)$ is the reacted fraction, and their corresponding application techniques are presented. When compared to the notations above, $X = 1 - X/c_0$ is assumed in [13], where X is the volume-averaged concentration **(1)** on the right. If only fractions appear in the model, then, when solving inverse problems of parametric identification from experimental data, no significant numerical dependence of K on the sample geometry (e.g., fine powder) and on the initial saturation level c_0 should be found. If such a dependence is observed, the authors recommend considering the hybrid model below. The dependence of the kinetic coefficient not only on the temperature T, but also on the parameters ℓ, c_0, is explicitly highlighted there. It is necessary to take into account what exactly is used as the phase variable X for the dynamical system of interest. In this paper, the remaining average concentration is used, as it clearly determines the further degassing rate.

We note the study [14] on powdered material (ErH3), which presents a relevant literature review. Models of powder particle dehydrogenation (high-temperature and diffusion peaks) are presented in [7]. In [15], the effect of initial saturation is analyzed in detail. The paper [16] contains an overview, a detailed description of the model proposed there, and an extensive list of references. Note also the detailed and thorough reviews with hundreds of references, including those on membrane technologies [17, 18].

3. Refinement of the kinetic coefficient

For now, we will consider an averaged model for diffusion and desorption processes for the volume-averaged concentration X

$$X \approx \ell^{-1} \int_0^{\ell} c(t,x)\, dx \Big|_{T(t)} = \bar{c}(T).$$

We choose, by virtue of $T(t,x) = T(t) = T_0 + \beta t$, $t \leftrightarrow T\ (t < t_{\max})$, the current temperature T as the independent variable. Shown in **(2)**, the Arrhenius dependence of the kinetic coefficient on T has so far only been postulated: $K(T)$. For porous, powdery materials, this can be limited to estimating the values of K_0 and Q from experimental data.

If we deal with metals and alloys, the model *must perceive* the geometry patterns (parameters ℓ, c_0). Let us represent this dependence in an explicit analytical form. Let us introduce the following notations:

$$K_D = \pi^2 D(T)\ell^{-2}, K_b = 2b(T)\ell^{-1},$$
$$D = D_0 \exp\{-E_D[RT]^{-1}\}, b = b_0 \exp\{-E_b[RT]^{-1}\}.$$

We set $K(T;\alpha,\ell) = K_D^{2-\alpha} \cdot K_b^{\alpha-1}$. Then, at $\alpha = 1$ we obtain K_D (diffusion limitation), and at $\alpha = 2$ we obtain K_b (desorption limitation). Intermediate values of α will correspond to a *mix* of volume and surface processes. The Arrhenius form in temperature will be preserved:

$$K(T;\alpha,\ell) = K_0 \ell^{\alpha-3} \exp\{-Q[RT]^{-1}\}, \tag{3}$$
$$K_0 = \pi^{2(2-\alpha)} \cdot 2^{\alpha-1} \cdot D_0^{2-\alpha} \cdot b_0^{\alpha-1},$$
$$Q = E_D(2-\alpha) + E_b(\alpha-1).$$

At fixed α, we have $K_0 = K_0(D_0, b_0)$ and $Q = Q(E_D, E_b)$. The parameter $\alpha \in [1,2]$ is informative: it shows in what proportion diffusion and desorption have shared their interdependent influence. The multiplier $\ell^{\alpha-3}$ is highlighted; therefore, the experiments on samples of different thicknesses are highly desirable. If there is no information on the values of the diffusion and desorption coefficients, then K_0 and Q in **(3)** can be considered as fitting parameters when approximating the experimental curves.

Let us note the following drawback, which we try to avoid. If we use dimensionless fractions

$$\tilde{X} \approx \frac{1}{\ell c_0} \int_0^{\ell} c(t,x)\, dx \Big|_{T(t)} \in [0,1],$$

then we obtain the approximation model

$$\frac{d\tilde{X}(T)}{dT} = -\frac{\overline{K}}{\beta} \tilde{X}^{\alpha}(T), \qquad \tilde{X}(T_0) = 1,$$
$$\overline{K} = K(T)\ell^{\alpha-3} c_0^{\alpha-1},\ K(T) = K_0 \exp\{-Q[RT]^{-1}\},$$
$$K_0 = K_0(\alpha, D_0, b_0) = \pi^{2(2-\alpha)} \cdot 2^{\alpha-1} \cdot D_0^{2-\alpha} \cdot b_0^{\alpha-1},$$
$$Q = Q(\alpha, E_D, E_b) = E_D(2-\alpha) + E_b(\alpha-1).$$

In the kinetic coefficient $\overline{K}$, the multipliers $\ell^{\alpha-3}$ and $c_0^{\alpha-1}$ are explicitly emphasized. For $K(T)$, we reserved the designation of the Arrhenius dependence on temperature. Parametric identification requires experiments not only at different ℓ but also at different initial saturation levels c_0. Therefore, it is preferable to operate with the volume-averaged concentration (without normalization) and use model **(2)** with $X(T_0) = c_0$ and the kinetic coefficient $K(T; \alpha, \ell)$ according to **Formula (3)**. The thickness of the sample is known, and the value of c_0 is determined after degassing.

Formally, this model is in the class of ordinary differential equations (ODEs) with separating variables and integrates in quadratures (but not in elementary functions). Further numerical integration of quadratures is not simpler than numerical integration of the original ODE, if we have common mathematical packages in mind (the authors used the freely available *Scilab*).

If there is no information about the values of D_0, E_D, b_0, or E_b, we take α, K_0, and Q as independent fitting parameters. A model in the form of a reaction of order $\alpha \in [1, 2]$ is only able to approximate the unimodal TDS spectrum $w(T) = -\dot{X}|_T = -\beta dX/dT$ (or the dependence $\widetilde{w}(T) = -d\tilde{X}/dt = -\beta d\tilde{X}/dT$). One can also plot $v(T) = -dX/dT$ if the dimension $[v] = 1/(\text{cm}^3\text{K})$ is preferred.

If the TDS spectrum $w(T)$ has several local peaks, one usually proceeds as follows. The dependence $w(T)$ is decomposed into the sum of reactions of first and second orders, and thereby a set of values of the pre-exponents K_0 and binding energies Q are estimated. Each local peak is interpreted as a release of hydrogen trapped by different types of traps. Formally, local reaction peaks are asymmetric [11], but often nearly symmetric with satisfactory accuracy. This allows us to automate the decomposition into the sum of reactions to be automated. In particular, one uses the decomposition of $w(T)$ into a sum of Gaussian curves in the *Origin* package.

In general, this is a significant mathematical problem. The decomposition of a function by powers of the argument is the theory of power series. The decomposition of a function by harmonics is the theory of Fourier series. Here, we are faced with a more difficult problem. The basic functions are the solutions of ODEs with separable variables. However, quadratures are not expressed in elementary functions.

4. A model with nonlinear dynamic boundary conditions

Let us proceed to a more detailed model, explicitly separating bulk and surface processes (following [19] (Chapter 6, pp. 177–208)). The vacuum system is considered powerful enough to neglect resorption. For a thin homogeneous plate of thickness ℓ under conditions of slow uniform heating, the boundary value problem of the TDS degassing takes the following form:

$$\begin{aligned}
&\partial_t c(t,x) = D(T)\partial_x^2 c(t,x), \quad t \in (0, t_*),\ x \in (0, \ell),\\
&\frac{dq}{dt} \equiv \dot{q}(t) = -b(T)q^2(t) + D(T)\partial_x c(t,0),\\
&c(0,x) = c_0,\ x \in [0,\ell], \quad c_{0,\ell}(t) = g(T)q(t),\\
&J(t) = b(T)q^2(t),\ T(t) = T_0 + \beta t,\ \beta > 0.
\end{aligned} \tag{4}$$

Here, $q(t)$ is the surface concentration ($1_{\text{H}}/\text{cm}^2$); $[c] = 1_{\text{H}}/\text{cm}^3$; D, b, and g are the Arrhenius temperature-dependent coefficients of diffusion, desorption, and rapid dissolution, and the dimensions of these coefficients are cm^2/s, cm^2/s, and $1/\text{cm}$; and $J(t)$ is the degassing (atoms recombined into molecules) flux density, $[J] = 1/(\text{cm}^2\text{s})$, where 1 denotes one H atom. We can obtain $J = J(T)$ by virtue of $t \leftrightarrow T$. Within the context of the model, the graph $(T, J(T))$ is the TDS spectrum. Let us emphasize that the surface is explicitly allocated. Therefore, desorption is assigned to the unit (cm^2) part of the surface. The total surface consists of two identical subsurfaces notionally named *left and right* ($S_1 + S_2 = 2S$). This should not be forgotten when recalculating the flux per unit of total area. The left and right subsurfaces will have the same concentration $q_{0,\ell}(t) = q(t)$ due to the symmetry of the experiment and the initial distribution.

The model "diffusion of atomic hydrogen in the volume lattice and desorption of molecular hydrogen from the surface" is adequate for materials with metallic properties (at not too high temperatures).

In the diffusion equation, it is taken into account that D does not depend on x, and it can be taken outside the sign ∂_x. To simplify the notation, we can use the short notations $D(t) \equiv D(T(t))$, $g(t) \equiv g(T(t))$, and $b(t) \equiv b(T(t))$. However, it should be borne in mind that the temperature is the argument of the coefficients. If the temperature is already very high and degassing is still significant, then further heating is usually discontinued ($T = T_{\max}$, $t > t_{\max}$), and the dependence $J(t)$ is analyzed in the following.

4.1. Comments, clarifications, and summaries

Remark. We assume a uniform initial distribution of concentration c_0. This requires the sample to be kept for a long time at a sufficiently high constant temperature and pressure of H_2. In terms of numerical methods, there is no problem with the value $c_0 = c_0(x)$. However, if we have the inverse problem of parametric identification in mind, then $c_0 = \text{const}$ is easily determined by the results of complete degassing of the sample, while the restoration of the function $c_0(x)$ is much harder. Moreover, if the distribution of $c_0(x)$ is asymmetric with respect to the centre of the plate thickness ($\ell/2$), then different sides will have different desorption fluxes, while only the sum is measured. If such an applied problem arises, there is no appreciable complication in the numerical solution of the direct problem when all the coefficients are given.

The experiment is symmetric. Thus, for a symmetric initial concentration $c_0(x)$ we have

$$c_0(t) \equiv c(t,0) = c_\ell(t) \equiv c(t,\ell), \qquad \partial_x c(t,0) = -\partial_x c(t,\ell).$$

The surface concentrations (at $x = 0, \ell$) are the same, and we use one notation $q(t)$ for the number of H atoms that are contained per cm^2 each of the two sides of the plate (the ends are neglected).

The surface is explicitly separated in the model. We leave the same notation $b(T)$ for the desorption coefficient. In the previous section (when desorption was strictly limited), it was the effective recombination (volume desorption) coefficient $b = b_{\text{volume}}$, $[b] = \text{cm}^4/\text{s}$. Now, it is the surface parameter $b = b_{\text{surface}}$, $[b] = \text{cm}^2/\text{s}$. Their interrelation is defined by the relation $b_{\text{surf}} = g^2 b_{\text{vol}}$.

The process of surface–volume interaction can be detailed:

$$\begin{aligned}
&k^-(T)[1 - c_{0,\ell}(t)c_{\max}^{-1}]q_{0,\ell}(t) -\\
&k^+(T)[1 - q_{0,\ell}(t)q_{\max}^{-1}]c_{0,\ell}(t) = \mp D(T)\partial_x c|_{0,\ell}.
\end{aligned}$$

The presence of the *threshold* factor $[1 - c/c_{\max}]$ leads to the following. If the concentration of H in the near-surface volume is close to the maximum possible, then dissolution essentially stops. The other multiplier is interpreted similarly, where the value

$\theta(t) = q/q_{\max}$ means the degree of surface occupation. We will focus on sufficiently high temperatures (hundreds of °C). Surface processes are activated much faster with the growth of T compared to diffusion. On a relative scale, we have $D\partial_x c \approx 0$ and, additionally, $q \ll q_{\max}$, $c \ll c_{\max}$. Then, we obtain $g = k^-/k^+$ ($c_{0,\ell}(t) = g(T)q(t)$). If the surface is isotropic (in the terms of $E_{k^-} \approx E_{k^+}$), then $g(T)$ depends weakly on temperature. The surface and volume concentrations *track* each other locally and rapidly. So one can consider $g = \text{const}$ within a sufficiently sharp local TDS peak.

Otherwise, there are four Arrhenius parameters in $k^{\pm}$, and the inverse problem of parametric identification becomes difficult to solve. It is necessary to keep in mind the limited informativeness of the TDS method and the need for unique estimation of parameters where applicable. After all, the results from thin plates are extrapolated to real structures (e.g., protective walls in ITERs). Thus, uniqueness of parameter values is necessary for proper revised estimation. Therefore, further on we will try to take into account only the most necessary characteristics of the considered dynamic processes. When borrowing values from the literature, one should keep in mind that, for example, the diffusion coefficient D obtained under different boundary conditions (in different boundary value problems) will have different values when processing the same experimental material. The *similarity* of models is necessary to compare the values of the parameters.

For a direct numerical modeling problem, an increase in the number of given parameters is not critical, since the boundary value problem is one-dimensional in spatial variables. This does not detract from its complexity, since we deal with non-standard nonlinear dynamic boundary conditions. A time derivative is present not only in the diffusion equation, but also in the boundary conditions. In generalized form, we have a functional differential equation (FDE) of the form $\dot{q}(t) = \mathcal{F}(t, q(t), q_{[0,t]}, \dot{q}_{[0,t]}, \dot{q}_{[0,t]})$. The current state $q(t)$ and the rate $\dot{q}(t)$ are affected not only by the background of $q_{[0,t]}$, but also by the background of the derivative $\dot{q}_{[0,t]}$. Formally, we obtain $\dot{q}_{[0,t]} = G(q_{[0,t]})$. But due to the incorrectness of the differentiation operation, the formal equation $\dot{q}(t) = \mathcal{H}(t, q(t), q_{[0,t]})$ will not have the properties of the operator $\mathcal{H}$ necessary for numerical analysis. Without dwelling on the analytical transformations, we only note that the *transfer* of the derivative in the right-hand side of the equation by means of the integration-by-parts operation leads to the occurrence of divergent series. In general terminology, such equations belong to the so-called neutral type and require the development of a more complex mathematical apparatus [20].

The actual TDS spectrum (the dependence of the desorption flux density $J(T)$ on the current temperature) often contains several local peaks. They are usually associated with different kinds of traps (material inhomogeneities) with different binding energies. However, at least a two-peak spectrum can also be described by a dynamical model in which there are no traps [6] (Figures 7 and 8). In the paper [6], a three-stage experiment "breakthrough–flow–thermodesorption" is implemented. This significantly increases the informative value of solving the inverse parametric identification problem.

In addition to traps, local peaks can be formed by the interaction between volume (diffusion without reversible trapping) and surface (desorption). Schematically, this occurs as follows:

1. Desorption from the surface and near-surface volume gives a local flux peak and depletes the subsurface layer of hydrogen, which further leads to a local flux drop.
2. During continued heating, diffusion intensifies in response to the large concentration gradient near the surface.
3. Atomic hydrogen influx from the volume generates an additional peak.

We emphasize that such a situation is numerically observed if the activation energies of diffusion and desorption are in ranges where neither of the factors is the only limiting one.

Of course, in reality, diffusion, desorption from the surface, and traps with different binding energies interact. This generates a multi-peak spectrum. The problem of distinguishing the physicochemical causes of local peaks arises.

Let us complicate the diffusion equation, taking into account reversible trapping in traps of different types (almost uniformly distributed in the volume, see [11] for more details):

$$\begin{aligned} \partial_t c &= D\partial_x^2 c - \sum_{\nu=1}^{m} \left[a_\nu^- [1 - Z_\nu] c(t,x) - a_\nu^+ z_\nu(t,x)\right], \\ \partial_t z_\nu &= a_\nu^-(T)[1 - Z_\nu] c(t,x) - a_\nu^+(T) z_\nu(t,x). \end{aligned} \tag{5}$$

Here, $z_\nu(t,x)$ are the concentrations of atomic hydrogen H ($1/\text{cm}^3$) trapped by defects of various types (microcracks, grain boundaries, etc.); $a_\nu^{\mp}$ are coefficients of H absorption and emission by traps (1/s); and $Z_\nu \equiv z_\nu(t,x)/\max z_\nu$.

Such a model contains too many parameters to guarantee the uniqueness of estimates from experimental data of limited informative value. The importance of solving the direct problem is that qualitative questions can be investigated, for example, what the sensitivity of desorption to variations in certain parameters and their combinations is. This problem is difficult to solve within mathematical packages because of the non-standardized boundary conditions. This overall impedes the application of algorithms for numerical modeling.

5. A hybrid model of thermal desorption

Let us turn to the main content of this paper. Let us set the problem of combining the two considered classes of models. The main mathematical complexity is related to the system of equations in partial derivatives. But the samples (plates) are usually thin. This leads to a reasonable experiment time and corresponds to the problems of membrane technologies. In particular, various alloys are investigated in order to increase the throughput for the extraction of particularly pure hydrogen from gas mixtures. Therefore, it is reasonable to move to volume-averaged concentrations.

In order not to clutter the calculations, we restrict ourselves to one type of trap (e.g., grain boundaries) with concentration $z(t,x)$. Let us write the diffusion equation

$$\partial_t c(t,x) + \partial_t z(t,x) = D(T)\partial_x^2 c(t,x), \quad T = T(t). \tag{6}$$

It is possible not to refer to the above model, but simply limit ourselves to material balance considerations: the change in total concentration $c + z$ is determined by the diffusion flux density $J_d = -D\partial_x c$. The diffusion **Equation (6)** follows from the continuity equation $\partial_t(c + z) = -\partial_x J_d$.

Let us integrate the **Equation (6)** over variable $x \in [0, \ell]$:

$$\int_0^\ell \frac{\partial c}{\partial t}\, dx + \int_0^\ell \frac{\partial z}{\partial t}\, dx \\ = \frac{d}{dt}\int_0^\ell c(t,x)\, dx + \frac{d}{dt}\int_0^\ell z(t,x)\, dx = D(T)\left[\frac{\partial c}{\partial x}\Big|_\ell - \frac{\partial c}{\partial x}\Big|_0\right].$$

Let us introduce volume-averaged concentrations

$$X(t) = \frac{1}{\ell}\int_0^\ell c(t,x)\, dx, \quad Y(t) = \frac{1}{\ell}\int_0^\ell z(t,x)\, dx.$$

By the symmetry $\partial_x c(t,0) = -\partial_x c(t,\ell)$, we obtain

$$\dot X(t) + \dot Y(t) = -2D(T)\frac{\partial c}{\partial x}\Big|_0 \cdot \ell^{-1}.$$

Here, we apply the expression for $D\partial_x c|_0$ to the equation for surface concentration **(4)**:

$$\frac{dq}{dt} \equiv \dot q(t) = -b(T)q^2(t) - \frac{\ell}{2}\left[\dot X(t) + \dot Y(t)\right].$$

And for the variables $X,\ Y$ we assume average models. For X,

$$\dot X(t) = -K(T)X^\alpha(t), \quad X(0) = c_0,$$
$$K(T) \equiv K(T;\ell,\alpha) = K_0\ell^{\alpha-3}\exp\{-Q[RT]^{-1}\}.$$

The values of K_0 and Q are determined by the balance of the diffusion–desorption interaction in accordance with the expressions in **(3)**. If there is no a priori knowledge of the orders $D_0,\ b_0, E_D,\ E_b$, we consider K_0 and Q to be variable fitting coefficients, as is α. Having estimated them from experimental data, we obtain information about the values of the quantities

$$D_0^{2-\alpha} \cdot b_0^{\alpha-1}, \quad E_D(2-\alpha) + E_b(\alpha-1).$$

The cases $\alpha = 1$ and $\alpha = 2$ are not excluded, and then we determine, respectively, the diffusion and desorption coefficients $D(T)$ and $b(T) = b_{\mathrm{vol}}(T)$ (see above). In this section, $b(T) = b_{\mathrm{surf}}(T)$. If $c(t,x) \approx c(t)$, $\alpha = 2$ (limiting by desorption), then

$$bq^2 = bg^{-2}g^2q^2 = bg^{-2}c^2 \Rightarrow b_{\mathrm{v}} = b_{\mathrm{s}}g^{-2} \Rightarrow b_{\mathrm{surf}}(T).$$

If a low-temperature peak is considered, one can fix $\alpha = 2$. At high temperatures, $\alpha = 1$. However, for such a choice there must be specific physical considerations about the material under specific experimental conditions.

The initial heating is less informative than the neighborhood of the TDS peak. We focus on the operating temperature range of 100–500 ℃ (for membrane technologies). Low and cryogenic temperatures are not considered. In our case, we assume that the traps are far from being filled, so that the value $z/z_{\max}$ can be neglected compared to 1 ($z/z_{\max} \ll 1$).

We now integrate over $x \in [0,\ell]$ the equation for z:

$$\partial_t z = a^-(T)c(t,x) - a^+(T)z(t,x),\ z(0,x) = z_0$$
$$\Rightarrow \frac{d}{dt}Y(t) = a^-(T)X(t) - a^+(T)Y(t),\ Y(0) = z_0.$$

Let us write the model in compact form. The dynamics of the concentrations (on the surface and in the volume) are as follows:

$$\begin{cases} \dfrac{dq}{dt} = -b(T)q^2(t) + \dfrac{\ell}{2}\left[K(T)X^\alpha(t) - a^-X + a^+Y\right], \\ \dfrac{d}{dt}X(t) = -K(T)X^\alpha(t), \quad K(T) = K(T;\alpha,\ell), \\ \dfrac{d}{dt}Y(t) = a^-(T)X(t) - a^+(T)Y(t). \end{cases} \tag{7}$$

The initial data (at uniform equilibrium initial saturation of the sample) are

$$q(0) = q_0, \quad X(0) = c_0, \quad c_0 = g(T_0)q_0,$$
$$Y(0) = z_0, \quad a^-(T_0)c_0 - a^+(T_0)z_0 = 0.$$

Note that the initial values of concentrations q_0, c_0, and z_0 are not independent within the model. In a direct numerical modeling problem, it is sufficient to set the value of q_0. The values of c_0, z_0 are determined by q_0 and coefficients $g(T_0)$ and $a^\pm(T_0)$. But when solving the inverse problem by the results of complete degassing, only the sum $2q_0 + \ell[c_0 + z_0]$ will be known.

Remark 4: Note that the change from the original boundary value problem **(4)** (with traps **(5)**) to the averaged model **(7)** reduced the dimensionality of the inverse parametric identification problem. This is natural due to the replacement of the distribution $c(t,x)$, which provides more complete information, by the averaged $X(t)$. We may introduce the parameter $\bar g$ from the condition $c_0 = \bar g q_0$ as a relation of the equilibrium concentrations after initial uniform saturation of the sample. The value of $\bar g$ depends not only on the material but also on $\bar p, \bar T$ (H_2 pressure and saturation temperature). We will not go into detail because the preliminary stage depends significantly on the specifics of the experiment and is formally outside the degassing model. Theoretically, the information $g(T(t))$ is not superfluous. It allows us to compare the near-surface volume concentration $c_{0,\ell}(t) = g(T)q(t)$ in the original boundary value problem with the averaged $X(t)$, estimating the degree of upward convexity of the distribution $c(t,x)$.

We are interested in the desorption flux density from the (two-sided) surface $J(t) = b(T(t))q^2(t)$. In axes (T,J), we have the TDS spectrum: a plot of the function $J(T)$ under monotonic heating when $t \leftrightarrow T(t),\ t \le t_{\max}$.

The first equation describes the dynamics of the surface concentration, which is affected not only by the current value of $q(t)$ itself, but also by the dynamics of the volume-averaged concentrations (diffusively mobile and trapped H atoms). The equation can be written as

$$\frac{d}{dt}\left[q + \tfrac{1}{2}\ell(X+Y)\right] = -b(T)q^2(t) \quad (b = b_{\mathrm{surf}}).$$

This is a material balance: except for the rate of change in the number of H atoms on the cm^2 surface (accumulation or loss at the surface), the total flux of H release is carried away by surface desorption from both sides of the plate.

Formally, we have a system of three ODEs (ordinary differential equations). But in truth, the equations are numerically integrated sequentially. First, we calculate $X(t)$ from the second equation. By applying it to the third equation, we obtain a linear ODE for $Y(t)$. These equations are integrated in quadrature, but for consistency it is better to use the procedures for the numerical integration of ODEs. With the known dependencies $X(t)$ and $Y(t)$, it remains to integrate the first equation for the concentration $q(t)$. It has quadratic nonlinearity (Riccati equation) and, in general, is not integrable in quadrature. We solve it numerically.

6. The initial simplifications of the computational scheme

Two extremes are described in Section 2 above: strict limitation by diffusion or desorption (recombination H+H=H$_2$). In this case, if $\alpha = 1$, then

$$K(T) = K(T;\ell) = K_D = \pi^2 D(T)\ell^{-2},$$

and the model **(7)** clearly includes the diffusion coefficient. The second equation does not include the effective recombination coefficient $b = b_{\text{vol}}(T)$. But the surface desorption coefficient $b(T) = b_{\text{surf}}(T)$ is present in the first equation, so that desorption is *not forgotten* and $b(T)$ is more informative, since it is introduced in a more accurate model with explicit surface separation. In the conventionally considered range 100–500 °C, it is mostly diffusion-limited. But there is an initial heating stage (T_0 typically room temperature). Diffusion equations *quickly forget* the initial data. This means that the initial data have a weak influence on the neighborhood of the desorption peak. Therefore, we limit ourselves to $\alpha \in [1, 3/2]$, starting the investigation from $\alpha = 1$ ($K = K_D$). As α increases, we take K_D as the initial approximation and shift slightly toward $K_b = 2b(T)/\ell$, $b = b_{\text{vol}}$.

If there are no order-of-magnitude estimates for D and b_{vol}, we are guided by **Formula (3)**, assuming that K_0 and Q are fitting parameters (however, we fix the multiplier $\ell^{\alpha-3}$). We can postulate the mean value $\alpha = 3/2$ right away. The parameter $g(T)$ depends weakly on T; hence, in the neighborhood of the TDS peak we assume $g = \bar{g} = \text{const}$ ($10^2 - 10^4$ 1/cm). For the averaged model, this is an independent parameter. It is indirectly related to the more accurate distributed model by the relation $\bar{g} = g(T_0)$.

The next simplification is as follows. The release of H from traps prevails under monotonic heating. We assume $a^- = \text{const}$ ($10^{-3} - 10^{-2}$ 1/s). And we consider the H release coefficient to be Arrhenius-dependent on temperature, with $a^- \ll a^+(T)$ at $T > 100$ °C. The value $E_a \equiv E_{a^+}$ is important for estimating the energy barrier of trap confinement. An obvious modification of **(7)** in the presence of different traps is to replace the third equation for $Y(t)$ by several single equations for $Y_i(t)$.

In general, the proposed model includes the range where diffusion in the volume and desorption from the surface significantly influence one another. From the computational point of view, the transition to volume-averaged concentrations in the lattice (diffusively mobile H) and in traps for thin sample plates allows us to operate not with a system of partial derivative equations, but with a consistently solved system of ODEs. This makes it possible to use any package of standard numerical methods, does not require specialized software, and allows us to quickly calculate the spectrum $(T, J(T))$ with minimum requirements for computing capacity.

Let us present the model for the initial numerical analysis, taking into account the simplifications adopted (the temperature-dependent parameters are the Arrhenius parameters):

$$\begin{cases} \dfrac{dq}{dt} = -b(T)q^2(t) + \frac{\ell}{2}[K(T)X^\alpha(t) - a^- X(t) + a^+(T)Y(t)], \\ \dfrac{d}{dt}X(t) = -K(T)X^\alpha(t),\ K(T;\alpha,\ell) = K_0\ell^{\alpha-3}\exp\Big\{-\dfrac{Q}{RT}\Big\}, \\ \dfrac{d}{dt}Y(t) = a^- X(t) - a^+(T)Y(t),\ a^- = \text{const}. \end{cases}$$

Initial data are the following: $g = \bar{g} = \text{const}$,

$$q(0) = q_0,\ X(0) = c_0,\ c_0 = \bar{g}q_0,$$
$$Y(0) = z_0,\ \ a^- c_0 - a^+(T_0)z_0 = 0.$$

There are independent varying parameters:

$$b = b_{\text{surf}}[b_0, E_b];\ \ell;\ \alpha \in [1, 3/2];\ \beta;\ K_0, Q;$$
$$[\alpha = 1 \Rightarrow K = K_D,\ K_0 = \pi^2 D_0,\ Q = E_D];$$
$$a^+[a_0^+, E_a];\ a^- = \text{const}[10^{-4} - 10^{-2}\ 1/\text{s}];$$
$$\bar{g} = \text{const}[10^2 - 10^4\ 1/\text{cm}];\ q_0\,[\Rightarrow c_0, z_0].$$

All parameters of the model b, K, α, $a^\pm$, and $\bar{g}$ have a meaningful physical meaning. The values K_0/ℓ^2 at $\alpha = 1$ (pre-exponent in $K(T)$) and $a^\pm$ are frequency factors (1/s).

7. The numerical modeling results

For certainty, we focus on published data for nickel and steel (12Cr18Ni10Ti grade) [21]. The parameter estimates depend significantly on the experimental conditions and sample preparation, so we take the values as modeling values for numerical illustrations. The general values are as follows:

$$\ell = 0.1\,\text{cm},\ T_0 = 300\,\text{K},\ \dot{T} = \beta = 0.5\,\text{K/s}.$$

The assumed parameter values for nickel are as follows:

$$b_0 = 3.4 \cdot 10^{-15}\,\text{cm}^2/\text{s},\ [E] = \text{kJ/mole},$$
$$E_b = 43,\ D_0 = 4.8 \cdot 10^{-3}\,\text{cm}^2/\text{s},\ E_D = 78,$$
$$g_0 = 20\,\text{cm}^{-1},\ E_g = 0,\ c_0 = 10^{18}\,\text{cm}^{-3}.$$

The parameters for steel are as follows:

$$b_0 = 5.05 \cdot 10^{-9}\,\text{cm}^2/\text{s},\quad E_b = 97.14,$$
$$D_0 = 3.09 \cdot 10^{-4}\text{cm}^2/\text{s},\ E_D = 27.78,$$
$$g_0 = 100\,\text{cm}^{-1},\ E_g = 0,\ c_0 = 9.96 \cdot 10^{17}\,\text{cm}^{-3}.$$

Using these parameters, we numerically plot the spectra (**Figure 1**) with the application of the model in the form of a boundary value problem **(4)** (curves with black circular markers). We emphasize that trapping is absent in the model. Nevertheless, two-peak curves are obtained: for nickel, the peaks are relatively isolated, while for steel the local maxima are pronounced but observed at relatively close temperatures. The same figures show the numerical spectra using the hybrid model (lines with black square markers). Varying the reaction order α in numerical experiments showed that $\alpha \sim 1$ should be used to approximate the two-peak spectra in the temperature range considered. The hybrid model without defects ($a^\pm = 0, z_0 = 0$) assumes a sequential solution of two ODEs: the first ($\dot{X} = \dots$) determines the dynamics of the volume-averaged concentration, and the second ($\dot{q} = \dots$) determines the desorption from the surface, taking into account the inflow of H atoms due to changes in the volume-averaged concentration. For steel (**Figure 1**, right), at the beginning of the experiment (300–470 K), there is a slight excess of influx from the volume to the surface (curve with white square markers) over the desorption flux. This leads to an initial increase in the concentration at the surface.

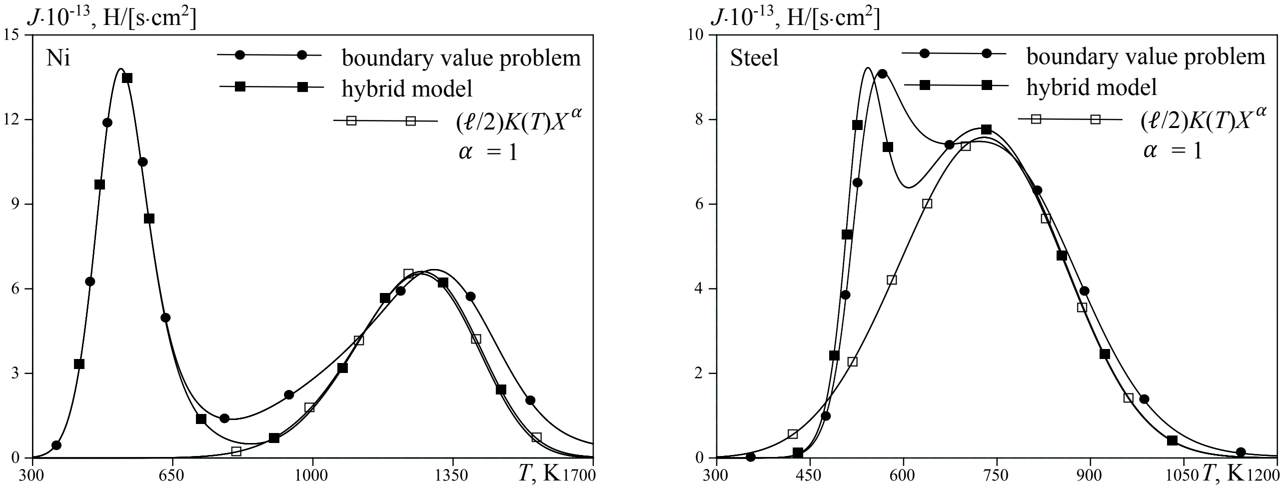

Figure 1 • Comparison of model fluxes: boundary value problem vs hybrid model.

For the numerical fluxes presented in **Figure 1**, we compare the averaged and boundary concentrations, see **Figure 2**. All concentrations are presented in fractions of the initial concentration. For the boundary value problem, we illustrate thickness-averaged concentrations (the curves with white circular markers) and boundary volume concentrations (the curves with black circular markers). For the hybrid model, volume-averaged concentrations (the curves with white square markers) and an analogue of the volume boundary concentrations (the curves with black square markers) are shown. In the hybrid model, there is no $c_{0,\ell}(t)$, and, in general, $gq(t)$ does not coincide with $X(t)$ at $t > 0$.

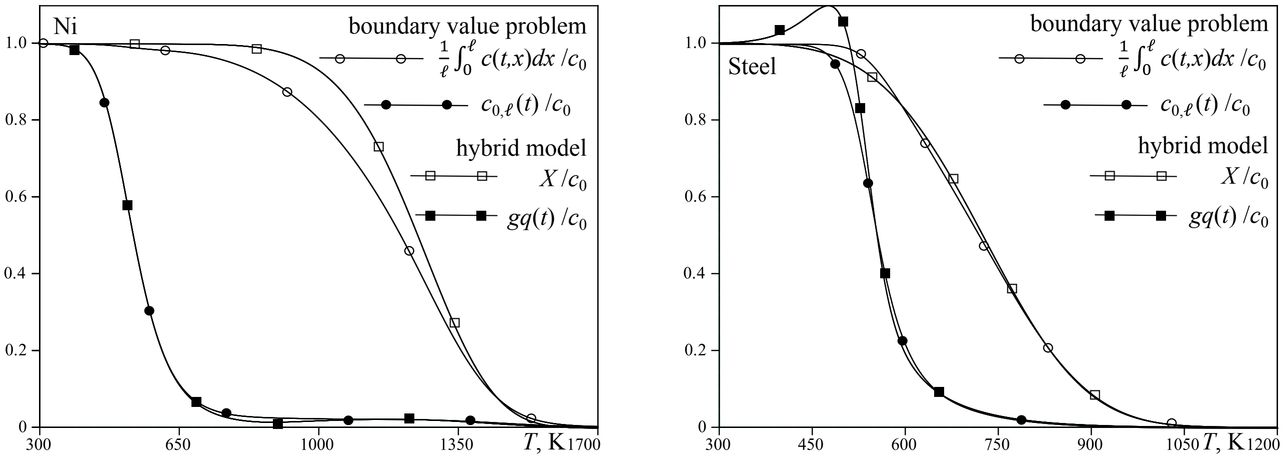

Figure 2 • Comparison of the model concentrations: boundary value problem vs hybrid model.

The figures show that at degassing under heating conditions, the boundary concentrations in the boundary value problem differ significantly from the averaged concentrations, i.e., the volume concentration profile $c(t, x)$ is not a horizontal *shelf*. The *gq* analogue boundary concentrations for the hybrid model (in the form of sequentially solved ODEs), in general, well approximate the boundary concentrations in boundary value problems with nonlinear dynamic boundary conditions. However, there is a possible effect when at the beginning of degassing the value of *gq* for the hybrid model increases slightly: the influx to the surface has already activated due to the changes in the averaged concentration, while desorption from the surface is still insufficient. As a result, we observe (**Figure 2**, right) a short-lived excess of *gq* of the initial level on the graph. Further, when degassing, the function *gq* in the hybrid model approximates well the boundary concentration $c_{0,\ell}$ of the boundary value problem. Comparing the averaged concentrations (the curves with white markers in **Figure 2**), close curves are observed in the figure on the right; on the left, the difference between the averaged concentrations is significantly greater. The reason for this lies in the larger curvature of the H concentration profile in the boundary value problem.

Figure 3 illustrates the effect of the reaction order α on the numerical spectra obtained using the hybrid model. The α values are given in decreasing order of maximums. At the beginning of degassing, a gluing of rising fronts is observed. The fractional value of α allows us to take into account the influence of surface processes and diffusion from the volume. Thus, at $\alpha = 1$ we observe two pronounced peaks: the first, low-temperature peak due to desorption from the (sub)surface, and the second, high-temperature peak due to inflow from the volume. As α increases, the degree of influence of the surface increases, and the second peak shifts to the lower-temperature zone. At $\alpha = 2$, the degassing process is strictly limited by the surface. We observe a single-peak (unimodal) spectrum with the largest peak flux. If we keep track of the decreasing α, we notice that bifurcation occurs with increasing influence (fraction) of diffusion: a two-peak structure emerges and develops. There are no traps in the model for now.

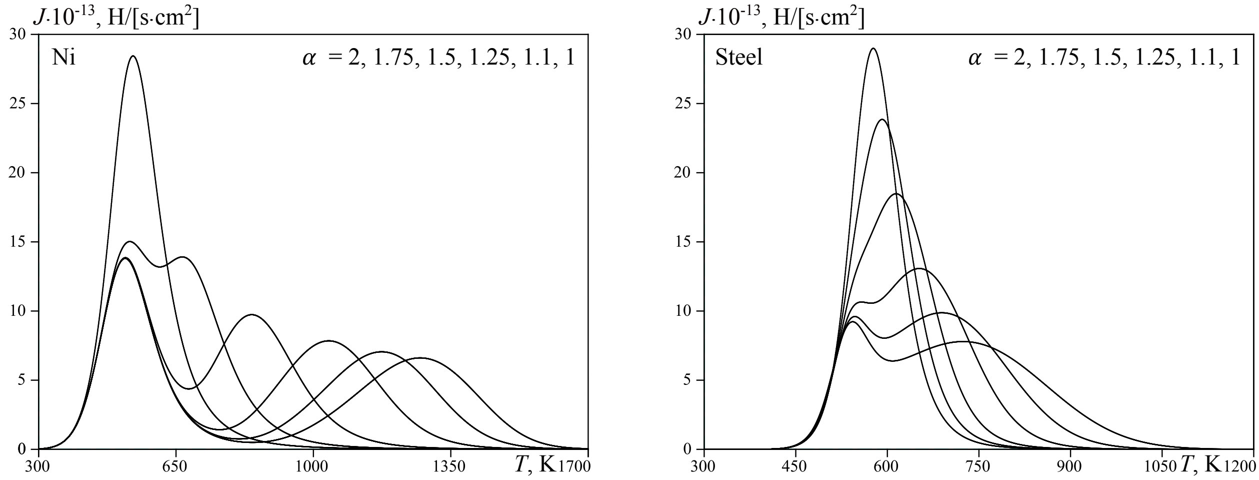

Figure 3 • Hybrid model, effect of α.

Figure 4 shows the flux plots in the overall flux balance at the surface (first equation of the hybrid model) due to changes in the averaged concentration. As the α parameter increases, the peak shifts to the low-temperature zone and becomes narrower. As α increases, the volume "empties" faster. As α decreases, we observe a more gentle rising front; diffusive inflow to the surface requires more heating to reach the peak value.

Let us illustrate the effect of parameters that can be varied in the experiment. **Figure 5** shows the change in the plots when the heating rate is varied. A lower heating rate corresponds to a spectrum with a smaller subgraph area. Material balance is obtained; however, the time of the experiment varies. The spectrum is a plot of $J(T)$, not $J(t)$. Qualitative changes in the spectra correspond to changes in the application of the model in the form of a boundary value problem.

Figure 6 shows the variation in the spectrum (hybrid model) when varying the initial concentration. As the initial concentration increases, more pronounced peak maxima are observed in the graphs.

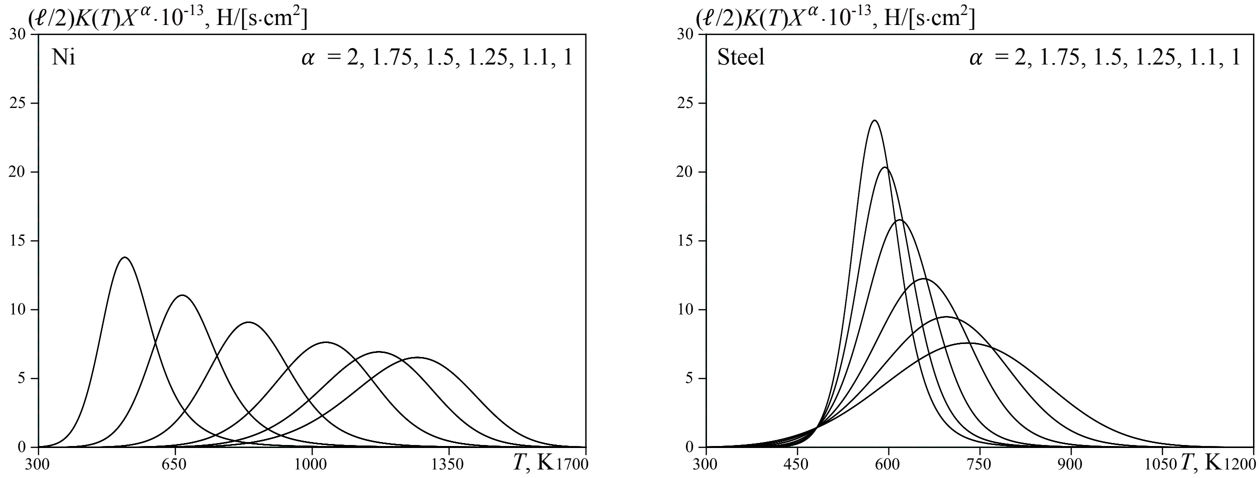

Figure 4 • Influx to the surface corresponding to a decrease in the averaged concentration.

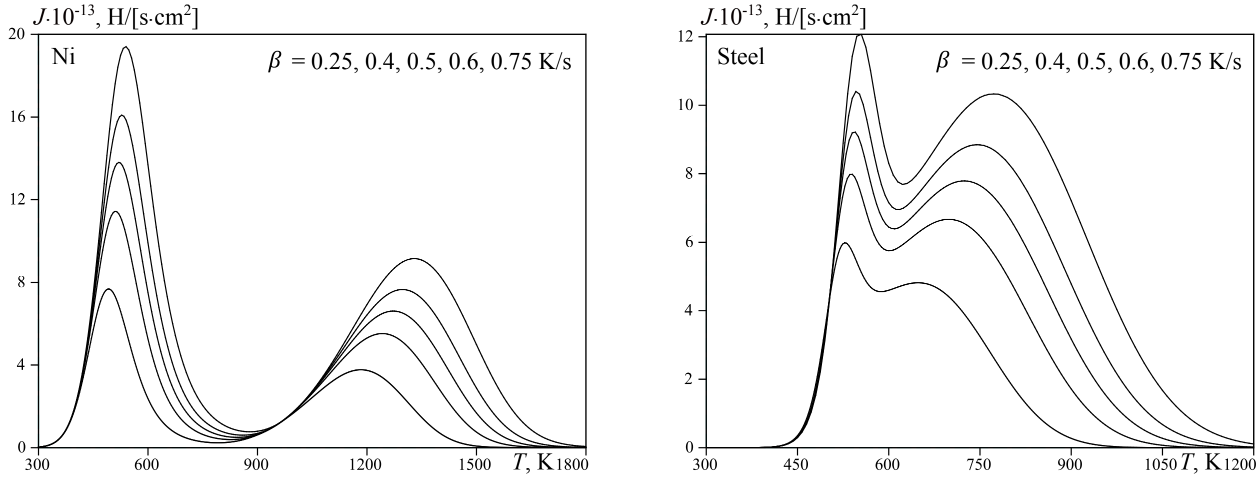

Figure 5 • Hybrid model, effect of heating rate.

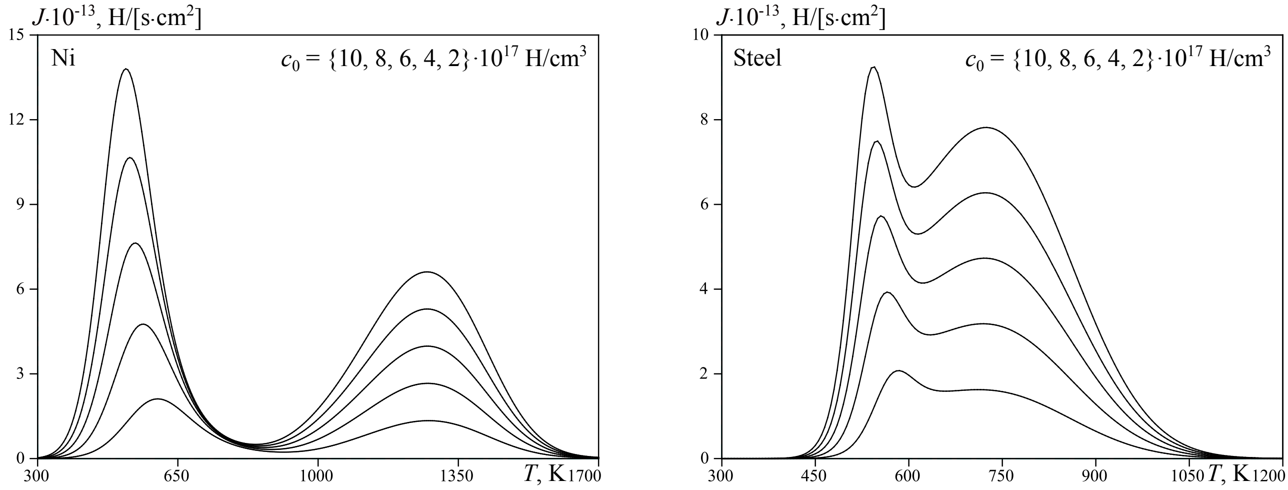

Figure 6 • Hybrid model, effect of initial concentration.

Figures 7–9 illustrate the effect of sample thickness on the spectrum. **Figure 7** shows the curves at $\alpha = 1$ when diffusion is limiting. The first and second peaks behave differently when the thickness is varied. As the thickness increases, the area of the second subgraph increases (it is proportional to ℓ). The maximum is reached at a higher temperature, because more time is required for diffusive influx to the surface. For steel (**Figure 7** right) at $\ell = 0.01$ cm, we observe one peak in the low-temperature zone, and the plate volume is negligible. At $\ell = 0.05$ cm, a low-temperature peak is observed at approximately the same temperature, but has a significantly larger peak value. There is no pronounced second peak yet: only a hint of a *shoulder* and a more gentle downward front. At $\ell = 0.1$ cm, isolated peaks are identified. The high-temperature peak becomes more pronounced. Varying the thickness of the sample allows us to distinguish the causes of the peaks, and see that the surface and diffusion peaks behave differently.

Remark 5: It is possible to approximate each peak separately by reactions of 1–2 orders (traps with different binding energies) in terms of volume-averaged concentration. Typically, the Gaussians sum decomposition in Origin is used. However, strictly speaking, the model reaction peaks are not perfectly symmetric. Then, the response of the peaks to the sample volume would be qualitatively commensurate. This is characteristic of powdery, porous materials. If the first peak is stable for a metal plate and the second peak significantly grows in terms of area with increasing ℓ, then this is in favor of the *surface–volume* interaction scenario from Section 4.1. A problem arises at the qualitative level, namely, how to distinguish between the scenarios, reversible trapping in traps or the interaction of desorption with diffusion, when neither factor is strictly limiting. The experiments with different ℓ allow us to clarify the picture. Naturally, in reality it is more complicated, especially for the multi-peak spectra with many different scenarios superimposed. This is a typical difficulty of the inverse problems. However, even for the two-peak spectra, the simulations show that the high quality of approximation alone is not sufficient to explain the physicochemical causes of peaks.

Figure 8 shows the change in spectra at $\alpha = 2$. The gluing of rising fronts is noted on the spectra. Desorption is strictly limited by the surface, and single-peak (unimodal) spectra are observed. In thin samples, the peak flux value is reached at lower temperatures.

Figure 9 illustrates the effect of sample thickness when fractional α is used in the hybrid model. For nickel (**Figure 9** on the left), surface processes play a major role ($\alpha = 1.75$). For steel (**Figure 9** on the right), the main contribution is made by the diffusion from the volume ($\alpha = 1.25$). Varying the plate thickness in the experim ent can help to reveal the physicochemical causes of the peaks.

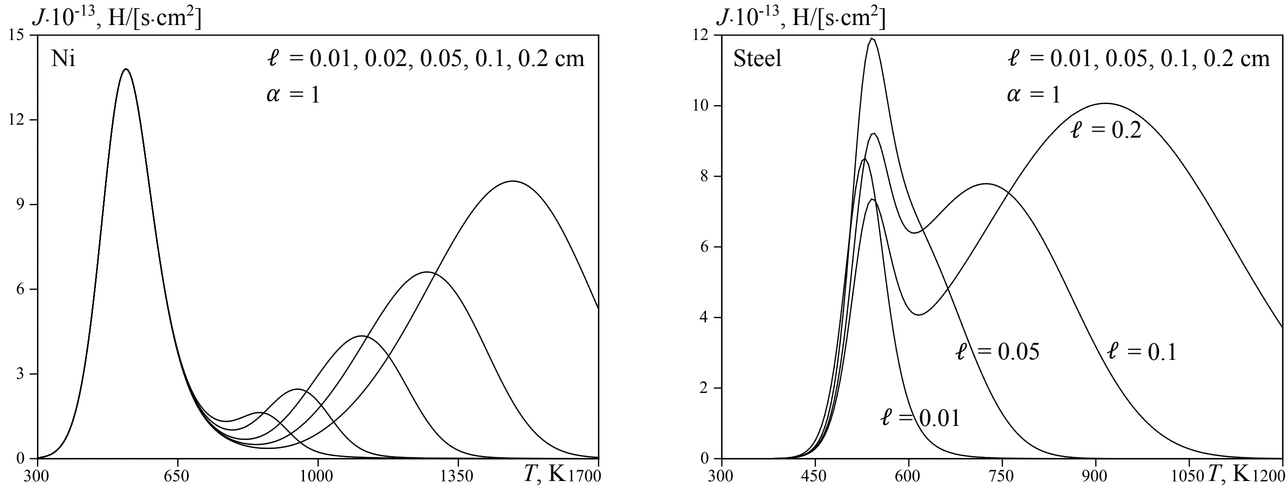

Figure 7 • Hybrid model, effect of sample thickness, $\alpha = 1$.

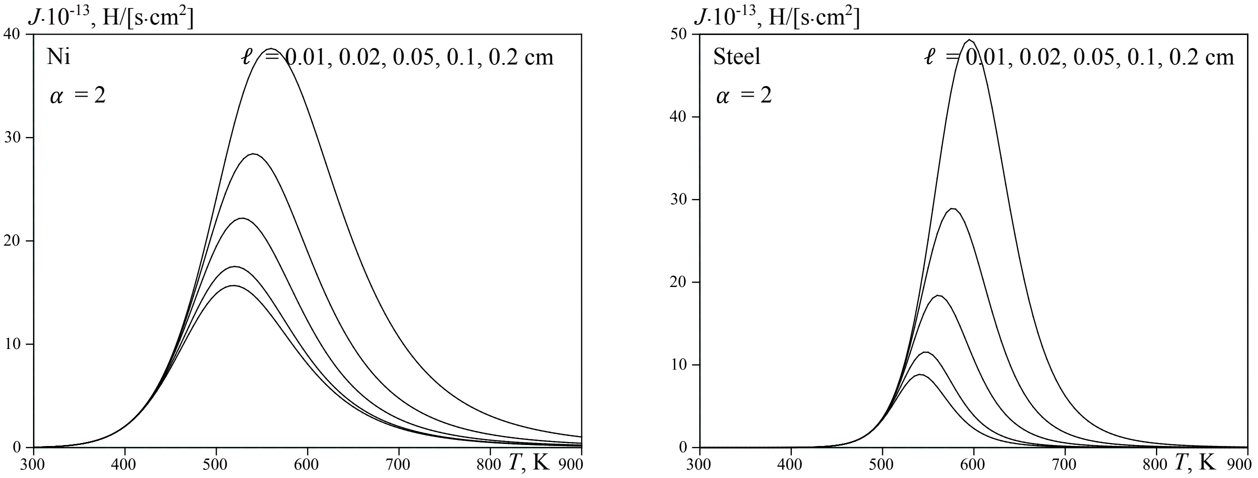

Figure 8 • Hybrid model, effect of sample thickness, $\alpha = 2$.

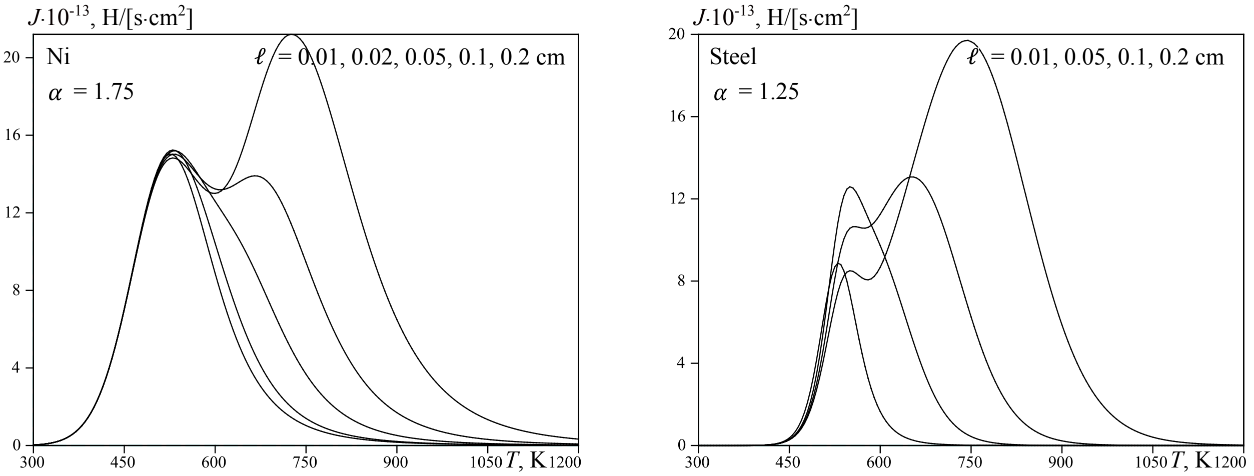

Figure 9 • Hybrid model, effect of sample thickness at fractional α.

Figure 10 shows the numerical spectra (boundary value and hybrid models) when defects are taken into account. **Figure 10** for nickel shows the spectrum, taking into account defects of "microcavity type" ($E_{a\pm} = 0$). The initial concentration of the defects is determined from the equilibrium conditions. Defects in the volume have a weak effect on the low-temperature surface peak. The influx from microcavity defects to the surface (curve with white rhombuses, **Figure 10** on the left) is intensified simultaneously with the influx to the surface, corresponding to a decrease in the volume-averaged concentration (curve with white squares). **Figure 10** on the right illustrates the effect of "hydride inclusion type" defects. Hydrogen release from the hydride begins when the temperature reaches 900 K. The flux from the defects is indicated by the white rhombuses in **Figure 10** on the right. This leads to a small jump in the thermodesorption flux for the hybrid model ($T = 900$ K, curve with black square markers) and a more gentle downward front. The taking into account of different types of defects is possible both in the model in the form of a boundary value problem and in the hybrid model. There are no fundamental difficulties: additional summands are added to the model and the technical calculations become only more lengthy.

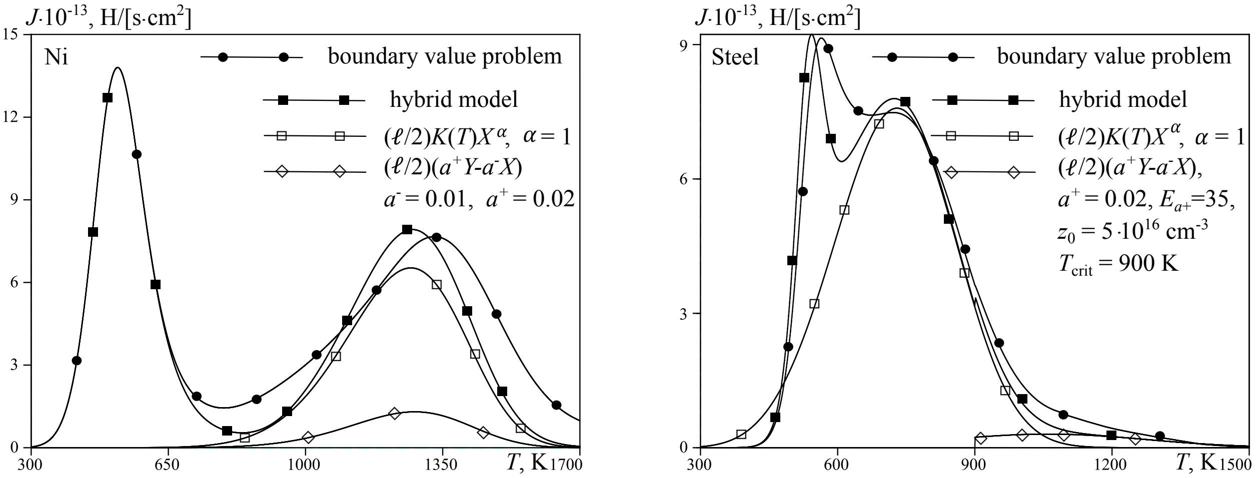

Figure 10 • Hybrid model, effect of defects: **left**—microcavity; **right**—hydride inclusions.

Figure 11 illustrates the decomposition of the two-peak numerical spectrum (boundary value problem without traps) into the sum of two reactions. The low-temperature peaks are well approximated by the second-order reaction, limited by desorption. At high temperatures, diffusion makes a larger contribution ($\alpha < 1.5$). The figures show the corresponding fractions of desorbed hydrogen (initial conditions) for each peak, the temperatures at which the flux maximum is reached, and the corresponding activation energies Q. The kinetic parameter K is not independent, $K = K(\alpha,\ T_{\max}, Q, \ell)$. What is the point of such a decomposition if the initial spectrum is based on a model without traps? We emphasize once again that the approximation does not solve the question of the physicochemical interpretation of the spectrum.

Figure 12 shows the variation in the model flux as a sum of two reactions when the heating rate is varied. The rising fronts of the low-temperature flux are glued together. The qualitative changes in the peaks are the same. Varying the heating rate does not unambiguously reveal the causes of the peaks. The differences in the area of the subgraphs are explained by different experimental times.

Figure 13 shows the change in the numerical spectra (sum of two reactions) when varying the initial concentration. The changes in the low-temperature and high-temperature peaks are similar. No noticeable shift in peak maximum temperatures is observed.

Figure 14 shows the effect of sample thickness on the model of the two-peak spectrum as a sum of reactions. On the left side of **Figure 14**, two relatively isolated peaks are observed for nickel. For the low-temperature peak, a gluing of rising fronts is noted. As the thickness increases, the flux maxima of the peaks increase, the temperature of the maximum of the second peak shifts towards higher temperatures, and the rising front of the second peak becomes more gentle. For steel, **Figure 14** on the right, one or two peaks are observed depending on thickness. At $\ell = 0.01$ cm, the flux intensifies faster (the rising front is steeper, the temperature of the flux maximum is smaller, and the peak flux value is small). The spectrum is single-peaked: the contribution of the second diffusion peak to the sum is hardly noticeable. As the thickness increases, the ($\ell = 0.05$ cm) becomes more pronounced, and then the second peak is isolated ($\ell \geq 0.1$ cm). It is interesting to compare these results with the plots in **Figures 7–9**.

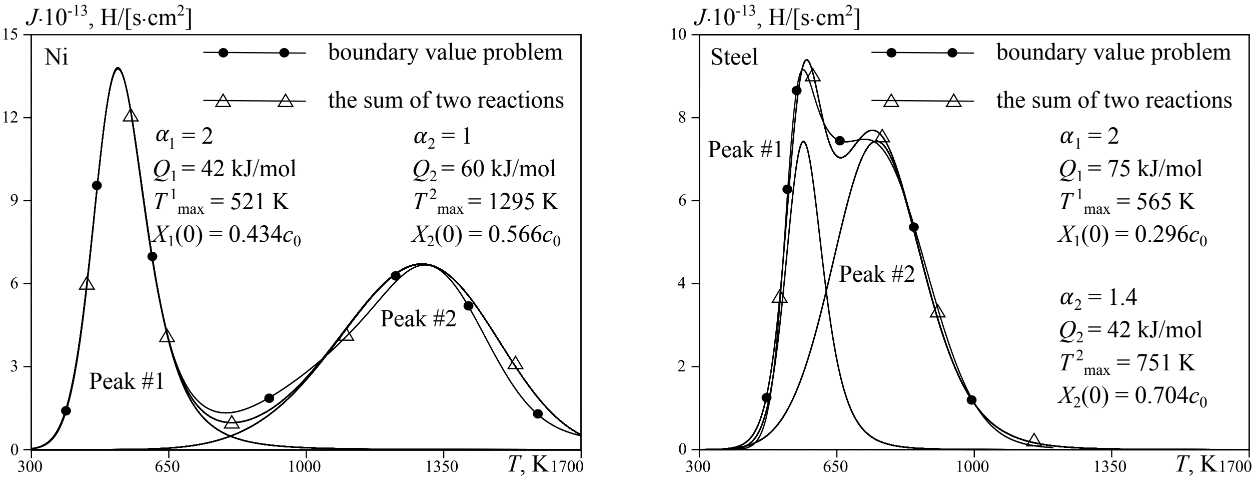

Figure 11 • Decomposition of the numerical spectrum (boundary value problem) into the sum of reactions.

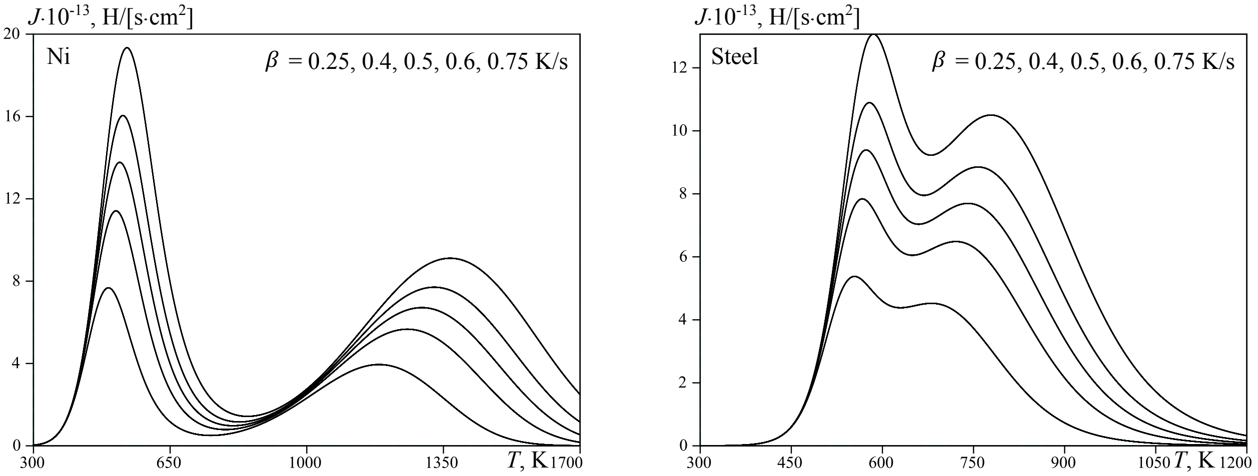

Figure 12 • Sum of reactions, effect of heating rate.

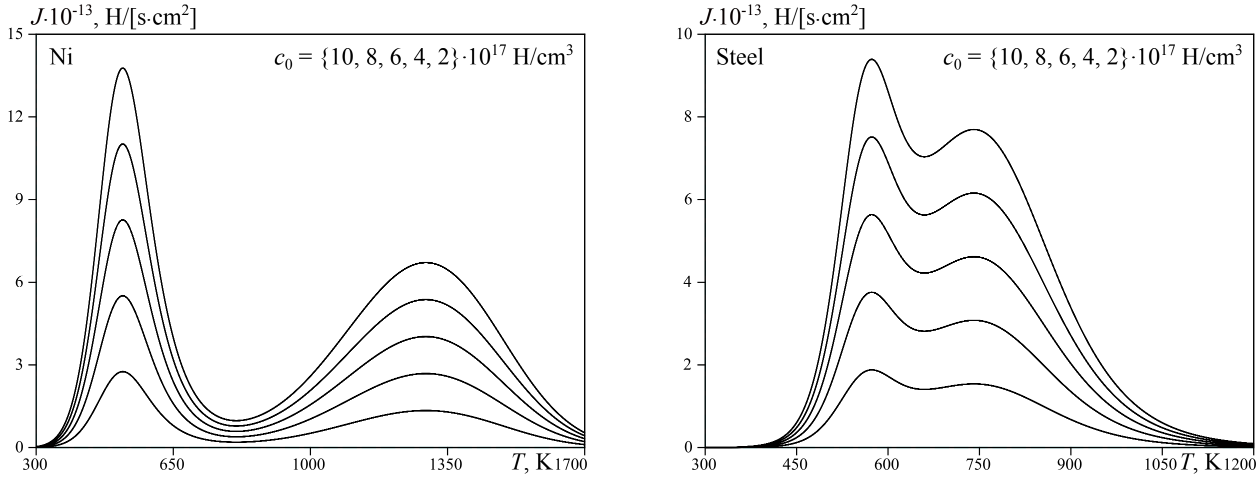

Figure 13 • Sum of reactions, effect of initial concentration.

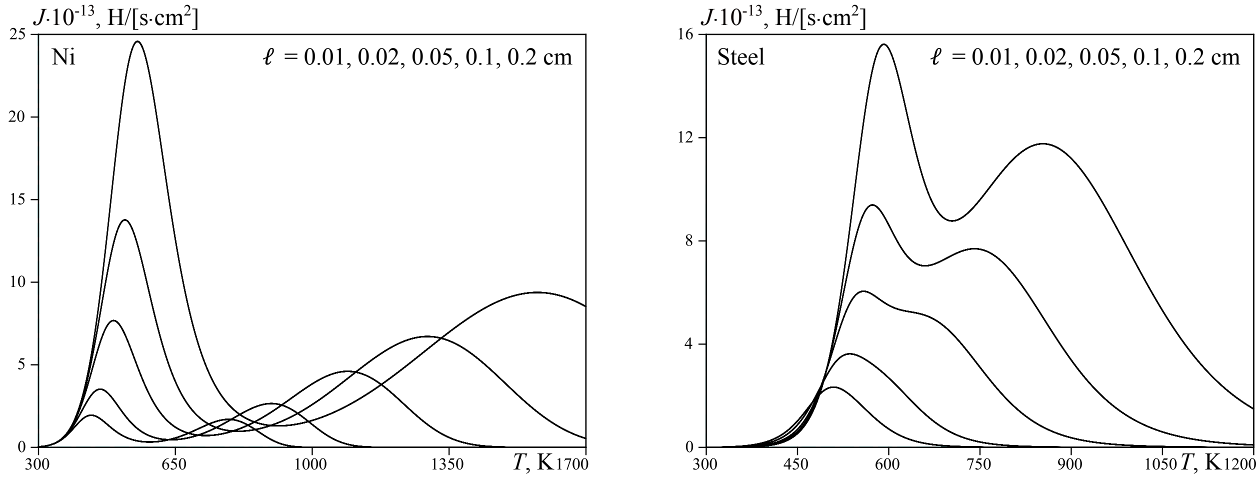

Figure 14 • Sum of reactions, effect of sample thickness.

8. Conclusions

The general conclusion from the computation results is as follows. The hybrid model has shown adequate consistency with physical representations both at qualitative and quantitative levels. In particular, it is possible to estimate the degree of influence of variations in various model parameters and experimental conditions on the degassing flux. Further, everything depends on the specific formulation of the applied problem and specific experimental material. If it is necessary to reveal qualitative differences at the level of *volume capture or surface dynamics*, then experiments with samples of different thicknesses are the most informative. We have materials with metallic properties in mind (an experimental test sample in the form of a thin plate), where it is possible to clearly identify both the volume and surface.

The model in a sense takes an intermediate position. Models in the form of first- and second-order reactions, often used in practice to decompose the spectrum into a sum of unimodal peaks, lead to quadrature. The main problem is decomposition by bases. The result is interpreted as the release of hydrogen trapped by different kinds of traps with different binding energies. This is not always valid, at least for metals and alloys.

The model in the form of a boundary value problem with dynamic boundary conditions is more detailed. Different stages and subprocesses of degassing are singled out: diffusion, dissolution, desorption, etc. But such a non-standard problem, when the time derivative is included not only in the diffusion equation, but also in the boundary conditions, requires special software.

The hybrid model combines the following. The model contains coefficients reflecting the processes of diffusion, dissolution, desorption, and reversible trapping by traps. However, instead of volume distribution, an averaged concentration is used. It is an acceptable approximation for thin membranes (plates). It allows us to fundamentally simplify numerical modeling as well as reveal the limiting factors in various applied problems. It is necessary to numerically integrate the low-order ODE system. This can be carried out in any package of standard mathematical programmes. In a short time (and without the need for programming), it is possible to accumulate large statistics in order to correct experimental studies. The estimation of parameters from data on thin samples allows us to recalculate the results for real structures and conditions not available in a real-time experiment.

Funding

The authors declare no financial support for the research, authorship, or publication of this article.

Author contributions

All authors have read and agreed to the published version of the manuscript.

Conflict of interest

The authors declare no conflict of interest.

Data availability statement

Data supporting these findings are available within the article, at https://doi.org/10.20935/AcadMatSci7591, or upon request.

Institutional review board statement

Not applicable.

Informed consent statement

Not applicable.

Additional information

Received: 2025-03-05

Accepted: 2025-03-28

Published: 2025-04-01

Academia Materials Science papers should be cited as *Academia Materials Science 2025*, ISSN 2997-2027, https://doi.org/10.20935/AcadMatSci7591. The journal's official abbreviation is *Acad. Mat. Sci.*

Publisher's note

Copyright

References

1. Yin S. Challenges and future directions for green hydrogen development. Acad Green Energy. 2025;2. doi: 10.20935/AcadEnergy7564
2. Vallejos-Romero A, Cordoves-Sanchez M, Cisternas C, Saez-Ardura F, Rodriguez I, Aledo A, et al. Green hydrogen and social sciences: issues, problems, and future challenges. Sustainability. 2022;15(1):303. doi: 10.3390/su15010303
3. Pleshivtseva Y, Derevyanov M, Pimenov A, Rapoport A. Comprehensive review of low carbon hydrogen projects towards the decarbonization pathway. Int J Hydrog Energy. 2023;48(10):3703–24. doi: 10.1016/j.ijhydene.2022.10.209
4. Guo L, Su J, Wang Z, Shi J, Guan X, Cao W, et al. Hydrogen safety: an obstacle that must be overcome on the road towards future hydrogen economy. Int J Hydrog Energy. 2024;51:1055–78. doi: 10.1016/j.ijhydene.2023.08.248
5. Zaika YuV, Sidorov NI, Rodchenkova NI. Aggregation of experiments for estimation of hydrogen permeability parameters. Int J Hydrog Energy. 2018;43:8333–41. doi: 10.1016/j.ijhydene.2018.02.137
6. Zaika YV, Sidorov NI, Fomkina OV. Identification of hydrogen permeability parameters of membrane materials in an aggregated experiment. Int J Hydrog Energy. 2020;45:7433–43. doi: 10.1016/j.ijhydene.2019.04.098
7. Zaika YV, Rodchenkova NI. Boundary-value problem with moving bounds and dynamic boundary conditions: diffusion peak of TDS-spectrum of dehydriding. Appl Math Model. 2009;33:3776–91. doi: 10.1016/j.apm.2008.12.018
8. Garcia-Macias E, Harris ZD, Martinez-Paneda E. TDS Simulator: a MATLAB App to model temperature-programmed hydrogen desorption. Int J Hydrog Energy. 2024;94:510–24. doi: 10.1016/j.ijhydene.2024.11.014
9. Shewmon PG diffusion in solids. Cham: Springer International Publishers; 2016. doi: 10.1007/987-3-319-48206-4
10. Crank J. The mathematics of diffusion. Oxford: Clarendon Press; 1975.
11. Zaika YV, Kostikova EK, Nechaev YS. Peaks of hydrogen thermal desorption: simulation and interpretation. Tech Phys. 2021;66(2):210–20. doi: 10.1134/ S1063784221020250
12. Pisarev A. Hydrogen gas-driven permeation through the membrane with asymmetric surface conditions. J Membr Sci. 2009;335:51–7. doi: 10.1016/j.memsci.2009.02.041
13. Lototskyy M, Denys R., Nyamsi SN, Bessarabskaia I, Yartys V. Modelling of hydrogen thermal desorption spectra. Mater Today. 2018;(5):10440–9. doi: 10.1016/j.matpr.2017.12.375
14. Ma M, Wang L, Wan R, Tang B, Tan X. Phase-structural transformation of erbium trihydride studied by thermal desorption spectroscopy. Int J Hydrog Energy. 2023;48(37):13913–21. doi: 10.1016/j.ijhydene.2022.12.328
15. Diaz A, Cuesta II, Martínez-Pañeda EM, Alegre Calderon JM. Influence of charging conditions on simulated temperature-programmed desorption for hydrogen in metals. Int J Hydrog Energy. 2020;45(43):23704–20. doi: 10.1016/j.ijhydene.2020.05.192
16. Polyanskiy V, Arseniev D, Chevrychkina A, Yakovlev Y. Hydrogen Skin Effect vs. Hydrogen Diffusion. Prog Contin Mech. 2023;196:377–410. doi: 10.1007/978-3-031-43736-6_22
17. Lider A, Kudiiarov V, Kurdyumov N, Lyu J, Koptsev M, Travitzky N, et al. Materials and techniques for hydrogen separation from methane-containing gas mixtures. Int J Hydrog Energy. 2023;48:28390–411. doi: 10.1016/j.ijhydene.2023.03.345

18. Lanjekar PR, Panwar NL. Hydrogen gas separation through membrane technology and sustainability analysis of membrane: a review. Emergent Mater. 2023;6:3. doi: 10.1007/s42247-023-00561-5

19. Zakharov AP, editor. Hydrogen interaction with metals. Moscow: Nauka; 1987. (In Russian)

20. Hale J. Theory of functional differential equations. New York/Heidelberg/Berlin: Springer-Verlag; 1977.

21. Yukhimchuk AA, editor. Isotopes of hydrogen. Basic and applied research. Sarov: RFNC-VNIIEF; 2009. (In Russian)